Published in final edited form as:
J Mol Cell Cardiol. 2011 January ; 50(1): 203–213. doi:10.1016/j.yjmcc.2010.10.003.

Fibronectin increases the force production of mouse papillary muscles via α5β1 integrin

Xin Wu[1], **Sanjukta Chakraborty**[1], **Cristine L. Heaps**[2], **Michael J. Davis**[3], **Gerald A. Meininger**[3], and **Mariappan Muthuchamy**[1]

[1]Department of Systems Biology and Translational Medicine, Texas A&M Health Science Center College of Medicine, College Station, TX 77843

[2]Department of Veterinary Physiology and Pharmocology, Veterinary College of Medicine, Texas A&M University, College Station, TX 77843

[3]Dalton Cardiovascular Research Center and Department of Medical Pharmacology and Physiology, University of Missouri-Columbia, Columbia, MO 65211

Abstract

The extracellular matrix (ECM) protein-integrin-cytoskeleton axis plays a central role as a mechanotransducing protein assemblage in many cell types. However, how the process of mechanotransduction and the mechanical generated signals arising from this axis affect myofilament function in cardiac muscle are not completely understood. We hypothesize that ECM proteins can regulate cardiac function through integrin binding, and thereby alter the intracellular calcium concentration ($[Ca^{2+}]_i$) and/or modulate myofilament activation processes. Force measurements made in mouse papillary muscle demonstrated that in the presence of the soluble form of the ECM protein, fibronectin (FN), active force was increased significantly by 40% at 1 Hz, 54% at 2 Hz, 35% at 5 Hz and 16% at 9 Hz stimulation frequencies. Furthermore, increased active force in the presence of FN was associated with 12–33% increase in $[Ca^{2+}]_i$ and 20–50% increase in active force per unit Ca^{2+}. A function blocking antibody for α5 integrin prevented the effects of the FN on the changes in force and $[Ca^{2+}]_i$, whereas a function blocking α3 integrin antibody did not reverse the effects of FN. The effects of FN were reversed by an L-type Ca^{2+} channel blocker, verapamil or PKA inhibitor. Freshly isolated cardiomyocytes exhibited a 39% increase in contraction force and a 36% increase in L-type Ca^{2+} current in the presence of FN. Fibers treated with FN showed a significant increase in the phosphorylation of phospholamban; however, the phosphorylation of troponin I was unchanged. These results demonstrate that FN acts via α5β1 integrin to increase force production in myocardium and that this effect is partly mediated by increases in $[Ca^{2+}]_i$ and Ca^{2+} sensitivity, PKA activation and phosphorylation of phospholamban.

Correspondence to: Mariappan Muthuchamy.

Disclosures: None declared

Keywords

Fibronectin; Integrin; Extracellular matrix proteins; Calcium; Force–$[Ca^{2+}]_i$ relationship; Phospholamban; Cardiac muscle

1. Introduction

Ventricular remodeling is the primary long-term adaptive mechanism in response to physiological (e.g. exercise) or pathological (e.g. diabetic cardiomyopathy) mechanical overload. In addition to hypertrophy of cardiac ventricular myocytes during mechanical overload, alterations in non-ventricular myocyte compartments, e.g. extracellular matrix (ECM), also form an essential component of the remodeling of the ventricle during diabetes mellitus and hypertension. ECM proteins communicate with intracellular molecules including cytoskeletal and Ca^{2+} signaling systems through integrins and are likely integrated with remodeling mechanisms. However, the mechanisms whereby integrin-ECM interactions are linked to mechanical signaling in cardiac muscle are poorly understood [1].

Integrins are a large family of transmembrane adhesion molecules that provide a connection between the intracellular cytoskeleton and ECM. Integrins are heterodimers composed of α and β subunits. Of the approximately 24 known integrins, cardiac myocytes express at least 4 prevalent subtypes, which include: α1β1, α3β1, α5β1 and α7β1 [2,3]. α3β1 binds to FN, collagen and laminin, whereas α5β1 binds most strongly to FN, α1β1 binds to collagen and laminin, and α7β1 binds to laminin [4]. The overlapping binding affinity between integrins and ECM proteins is likely due to common binding motifs, for example, arginine–glycine–aspartic acid (RGD) and leucine-aspartate-valine (LDV) amino acid sequences present in many ECM proteins. α1β1, α3β1 and α5β1 recognize ECM proteins that are containing RGD sequences [2,5]. In cardiac muscle, integrins localize in costameres, the sites where *Z* bands connect to basement membrane. The costamere is structurally integrated with cytoskeletal components and signaling complexes further supporting the proposition that integrins are involved in mechanical signaling [1,3,5–7]. It has been reported that application of mechanical stress to integrin adhesion sites causes increased cytoskeletal stiffening, generation of second messenger signals and tyrosine phosphorylation of proteins anchored to the cytoskeleton [8–10]. Thus, there is a strong evidence to suggest that integrins can act as a conduit for transmission of mechanical forces across the cell membrane and thereby initiating intracellular signaling.

Intracellular Ca^{2+} handling mechanisms include Ca^{2+} entry, Ca^{2+} release and Ca^{2+} reloading of the sarcoplasmic reticulum (SR). We have previously shown that at least 3 different integrins regulate voltage-gated L-type Ca^{2+} channels (Ca_L) and Ca^{2+} activated K^+ channels in native vascular smooth muscle (VSM) cells, neuronal cells, and in heterologously expressed neuronal, VSM or cardiac Ca_L in human embryonic kidney (HEK) −293 cells. Regulation of the ion channels by integrins requires signaling between focal adhesion proteins [11–17]. Numerous studies have indicated that alterations in Ca_L and $[Ca^{2+}]_i$ are primary mechanisms for the cardiac hypertrophic response [18–22]. Rueckschloss and Isenberg have reported contraction–induced enhancement of Ca_L in guinea-pig cardiomyocytes attached to coverslips coated with either FN or RGD containing peptides [23]. We have demonstrated that RGD-containing peptides or digested fragments of collagen depress force production by mouse papillary muscle fibers [2]. Since the binding affinities between different ECM proteins and integrins are varied, we propose that the downstream mechanical signaling will also be different and will depend upon the specific ECM proteins and integrins involved.

FN is normally expressed in the heart and undergoes increased expression in hypertrophic and injured myocardium [7,24–27]. These studies address the role of FN in the structural remodeling that occurs in hypertrophic or injured hearts. However the role of soluble FN in normal heart function is poorly understood. Laser et al. have suggested that increased FN expression in feline myocardium during hypertrophy may involve focal complex formation and the activation of extracellular-regulated kinases 1/2 following α5β1 integrin binding [28]. In this study we test the hypothesis that soluble FN interacts with α5β1 integrin to augment force development by altering $[Ca^{2+}]_i$ and myofilament activation processes.

2. Materials and methods

2.1. Force measurements in intact papillary muscle fibers

Adult male mice (FVB/N strain, 15–20 weeks, 25–35 g, Harlan Houston, TX, and Charles River, USA) were anaesthetized by an intraperitoneal injection of sodium pentobarbital (60 mg/kg) and hearts were excised rapidly. The hearts were placed in cold (4 °C) Krebs-Henseleit (KH) buffer containing 10mM 2, 3-butanedione monoxime (Sigma, USA). KH buffer was composed of (in mM): 119.0 NaCl, 11.0 glucose, 4.6 KCl, 25.0 $NaHCO_3$, 1.2 KH_2PO_4, 1.2 $MgSO_4$ and 1.8 $CaCl_2$. The buffer solution was gassed with 95% O_2–5% CO_2 to maintain the pH (7.35–7.40). The right ventricular papillary muscle (2.0 – 3.0 mm in length, 0.3–0.4 mm in width and 0.15–0.25 mm in thickness) was isolated by dissection with a segment of the tricuspid valve at one end and a portion of the myocardial septum at the other. The muscle tapered from the ventricular wall toward the attachment to the tricuspid valve such that the shape approximated that of a triangle with length and with an oval base width. The force was normalized per cross-sectional area at the base using the approximation area=0.75 × width × depth [29]. The papillary muscle bundles were mounted between a force transducer and a voltage-controlled motor positioner within a muscle measurement suite (Scientific Instruments, Germany). Stimulation pulse duration was 6 ms with an initial rate of 1.0 Hz. The papillary bundle was continuously superfused with KH maintained at 37 °C for force measurement. Stimulation voltage and bundle length were adjusted until maximum force was reached. The muscle was then stimulated at 1.0 Hz for 20–30 min before executing the experimental protocol. A digital phosphor oscilloscope suite (Tektronix TDS 420A with Wavestar software) measured stimulation frequency, twitching force amplitude, averaged force amplitude within preset time windows, and continuously logged the data into the computer.

The experimental protocols consisted of: (1) increasing stimulation frequency by 1.0 Hz increments (duration of 2 min or until a steady force value had been reached); (2) decreasing stimulation frequency to a randomly selected frequency (5.0 or 1.0 Hz) and superfusing with KH solution containing either 35.0 nM FN (440 kD, Invitrogen Corporation, Grand Island, NY) or 35.0 nM bovine serum albumin (BSA. Amersham Life Science, Arlington Heights, IL) for 5 min before starting to record data; (3) in experiments with integrin-blocking monoclonal antibodies (mAb), the preparations were incubated for 5 min with α5 (HMα5–1, 60 nM) or α3 (VLA-3α, 60 nM) mAb (BD Bioscience, San Jose, CA) prior to perfusion with FN, and (4) for inhibitor studies, the papillary muscle fibers were incubated with either the cardiac selective Ca^{2+} channel blocker 2.5 μM verapamil or the cell-permeable PKA inhibitor 14–22 amide (PKA-I, 1 μM. Calbiochem, Gibbstown, NJ) for 5 min before application of FN. Chemicals, unless otherwise stated, were obtained from Sigma.

Preparation of FN: FN (5.0 mg) was reconstituted, according to the manufacture's (Invitrogen Corporation, Grand Island, NY) manual, by adding 5 ml of sterile distilled water. The resulting solution was 1 mg/mL of FN in 100 mM CAPS, 0.15M NaCl, 1 mM calcium chloride, pH 11.5, and the concentration of FN in this stock solution was 2.3 μM. The FN stock solution was then filtered through Ultrafree-MC centrifugal filter to remove

any particles and/or precipitates that may present in FN. Then about 100 μl to 500 μl aliquots of FN was stored at −20°C in small plastic silicon ized tubes till the use in experiments; repeated freezing and thawing of the stock solution was avoided. 300 μl of FN stock solution was added directly to 20 ml Krebs-Henseleit (KH) solution before each experiment, which yielded the desired final concentration of FN (about 35 nM); the pH was adjusted to 7.4, and used in the experiments as described above. Similar protocol was also done for BSA in KH solution.

2.2. Force– Ca^{2+} measurements in intact papillary muscle fibers

Right ventricular papillary muscle bundles were extracted and mounted as previously described. The muscle measurement equipment suite provided all the optics and electronics needed for measuring $[Ca^{2+}]_i$ using Fura-2 AM dye. Measurements were collected through a different data acquisition suite (National Instruments A/D board and LabVIEW software, Austin, TX) with the digital oscilloscope suite providing continuous monitoring. A mercury lamp and filter wheel provided alternating ultraviolet (UV) pulses of 340 nm and 380 nm at 250 Hz with pulse duration of 1.5 ms to illuminate the bundle. The combinations of microscope, dichroic mirror, filter and photomultiplier tube collected the Fura-2 fluorescence. A synchronized electronic integrator parsed and averaged the respective fluorescence signals associated with 340 nm and 380 nm excitation. The loading solution consisted of KH with 10 μM Fura-2 AM (Invitrogen/Molecular Probes, Eugene, OR), 4.3 mg l–1 N,N,N',N'-tetrakis (2-pyridylmethyl) ethylenediamine, and 5.0 g/L cremophor. The KH to dimethyl sulfoxide volume ratio of the loading solution was 333:1. A loading duration of 1.5 h with 20 min of de-esterification gave signals of greater than 3-fold over background fluorescence. The ratio, R, of fluorescence from 340 nm excitation to fluorescence from 380 nm excitation was calculated after subtracting background fluorescence. Ca^{2+} concentration was calculated using the following equation with K_d equating to Kd x β after subtracting background fluorescence [30]:

$$[Ca^{2+}]_i = K_d * [(R - R_{min})/(R_{max} - R)] * \beta$$

where β is the ratio of the 380 nm signal at zero Ca^{2+} versus the 380 nm signal at saturating Ca^{2+} (39.8 μM). The ratio of 340/380 fluorescence was converted to $[Ca^{2+}]_i$ using a standard method [30]. The minimum ratio (R_{min}) was determined in zero Ca^{2+} with 10 mM EGTA and the maximum ratio (R_{max}) was determined in 39.8 μM Ca^{2+}. The experimental protocols were the same as described in the earlier section except that the protocols were carried out at room temperature. Myocytes increase their ability to actively pump out the Ca^{2+} sensitive dye Fura-2 with increasing temperature. At near physiologic temperature, the myocytes will actively eliminate enough Fura-2 such that additive noise becomes a confounder. The ratio method of Fura-2 eliminates similar multiplicative noise but does not remove the additive noise. Thus, it was not possible to load the Fura-2 into myocyte using our current protocol to conduct the force/frequency with Ca^{2+} experiments at near physiologic temperature. However, at room temperature the Fura-2 dye load into myocytes more efficiently and it is possible to measure force and Ca^{2+} simultaneously.

2.3. Analyses of the force–Ca^{2+} data

From the Ca^{2+} and force values, time-to-peak Ca^{2+} amplitude and time-to-peak force (TPF), and time from peak Ca^{2+} to peak force and the maximum rate of isometric tension development [+d*F*/d*t*, (mN/mm^2)/s)] represented contraction properties. The 50% decay time from the peak of Ca^{2+}, the 50% relaxation time from the peak of force, and the maximum rate of relaxation [−d*F*/d*t*, (mN/mm^2)/s] represented relaxation properties. The

+dF/dt and −dF/dt were calculated using the following equation, where $F(t)$ was the measured force at a particular time t and ΔT was the 1 ms sampling period:

$$dF/dt=[F(t-\Delta T)-F(t)]/\Delta T$$

Averaging a three data point window for each single dF/dt calculation minimized the noise. Data analyses were performed as described in our previous publications [31,32]. We analyzed the force– Ca^{2+} values at specific points during a twitch cycle. The points consisted of: (1) the resting point '*A*', (2) maximum Ca^{2+} point, '*B*', and (3) maximum force point, '*C*'. Active force, $[Ca^{2+}]_i$ and active force/delta gain of $[Ca^{2+}]_i$ were calculated at points *A*, *B* and *C*.

2.4. Adult cardiomyocyte preparation

Adult male mouse cardiomyocytes (FVB/N strain, 2–4 months) were prepared as described [3]. Briefly, the heart was harvested under anesthesia and put into ice-cold Ca^{2+} free physiological saline solution (PSS) containing (in mM): 133.5 NaCl, 4 KCl, 1.2 NaH_2PO_4, 1.2 $MgSO_4$, 10 HEPES, and 11 glucose, pH 7.4. 10 mM 2,3-butanedione monoxime (BDM) was present during the dissecting procedure. The aorta was cannulated and the heart was mounted in a Langendorff perfusion system with Ca^{2+}-free control solution containing 1 mg/ml bovine serum albumin (BSA, Amersham Life Science, Arlington Heights, IL) at 37 °C . Perfusion was continued with the same solution containing 25 μM Ca^{2+} together with collagenase type I (62.4 U/ml, Worthington, NJ) and type II (73.7 U/ml, Worthington, NJ). After about 15 –20 minutes, the heart was removed and transferred to a Petri dish containing PSS with 100 μM Ca^{2+}. The ventricles were cut into small pieces that were then gently triturated to release single cells. The collected cells were then re-suspended in PSS containing 200 μM Ca^{2+}. A suspension of freshly dispersed cells was plated onto a dish for at least 30 min in PSS solution with 1.8 mM Ca^{2+} before beginning the experimental protocols.

2.5. Electrophysiology

Whole-cell currents were recorded using Axopatch 200B, Digidata 1322A and pCLAMP9 software (Axon/Molecular Devices, Sunnyvale, CA). All experiments were performed at 22 °C. Conventional whole-cell recording s were made as described previously [12,33]. Pipettes had resistances ranging from 1 to 5 megaohms. The extracellular solution contained (in mM): 135 TEA-Cl, 1.1 $MgCl_2$, 2 $BaCl_2$, 10 glucose, 10 HEPES, 10 4-aminopyridine, 0.01 TTX (pH = 7.4). The intracellular solution (high Cs+) contained (in mM): 110 CsCl, 20 TEA-Cl, 10 EGTA, 10 HEPES, 2 $MgCl_2$, 4 Mg-ATP, 1 $CaCl_2$ (pH=7.2). These solutions provided isolation of Ca^{2+} currents (I_{Ca}) from other currents and from the Na^+-Ca^{2+} exchanger. Ba^{2+} in extracellular solution served as the charge carrier to increase the size of the inward currents elicited by depolarization, and to minimize Ca^{2+}-dependent inactivation of I_{Ca} [11,12]. I_{Ca} of cardiomyocytes was elicited by voltage ramps or by voltage steps from −60 to +40 mV in 10 mV increments every 5 sec at holding potential = – 50 mV.

2.6. Measurements of cell contractions

Two parallel platinum electrodes 5 mm apart were placed on each side of cardiomyocytes. The isolated myocytes were field stimulated at 1 Hz with a biphasic square pulse of 8 ms total duration. The amplitude and duration of the pulses were controlled by a SD9 Grass stimulator (Grass Technologies, MA). The stimulus amplitudes were set to 20% above threshold. Cell images were acquired through a Olympus CKX41 inverted microscope (at ×400 magnification) using a Hitachi charged-coupled device color camera, and video acquisition card (PCI 1409; National Instruments). The cell contraction tracking program

was written in LabView, with subroutines called from the supplemental IMAQ Vision Development Package (National Instruments, Austin, TX) [34].

2.7. Western blot analysis

Papillary fibers were stimulated at 3.0 Hz, either in the absence or presence of FN, at 37°C for 4 mins. The fibers were then flash-frozen in liquid nitrogen and stored at−80°C until use. Lysates were prepared by homogenizing the tissue in ice-cold RIPA lysis buffer supplemented with phosphatase inhibitors and protease inhibitor cocktail (Sigma, MO), as described earlier [35]. The tissue samples were then further sonicated in protein-solubilizing buffer. The supernatant was assayed for protein concentration, mixed with an equal volume of SDS gel-loading buffer [36], and run on a 4–20% precast gradient SDS-polyacrylamide gel (Bio-Rad Laboratories). For analysis of total phospholamban (PLB) and phospho-phospholamban (p-PLB) expression, both the control and FN-treated samples in SDS gel loading buffer were either boiled for 3 mins or were heated at 37°C for 15 mins prior to loading [37]. The proteins were transferred to a nitrocellulose membrane with a Bio-Rad transblot apparatus and the transfer was verified by Ponceau-S staining. The membrane was blocked in 5% milk in Tris buffered saline (TBS) and then incubated with a primary antibody followed by incubation with the corresponding HRP-conjugated secondary antibody. The following dilutions of the primary antibodies in TBS were used: PLB (1:1000) and anti-p-PLB Ser16 (1:1000), (Upstate Biotechnology, VA), GAPDH (1:5000) (Millipore, MA), phospho-TnI Ser23/24 (1:1000) (Abcam, MA) and TnI (1:4000) (Advanced Immunochemical, CA). The immunoreactive bands were visualized using the Pierce detection system (Super Signal West Dura Extended Duration Substrate, Pierce). Membranes were stripped by incubation in Restore western blot stripping buffer (Thermo Scientific, MA) and re-probed with the corresponding total antibody or GAPDH (1:1000). Densitometry analyses on the resulting bands were performed using Quantity One multi-analyst software (BioRad, CA). The ratios of p-PLB were calculated with respect to both PLB and GAPDH, and the ratio of phosphorylated cardiac troponin I (p-TnI) and total troponin I (TnI) was also calculated. Each experiment was repeated three times.

2.8. Statistical analyses

All data are expressed as means ± SEM. Statistical analyses were done using either a Student’s paired t-test or a two-way ANOVA with Fisher’s or Bonferroni/Dunn’s post hoc tests. Repeated measures ANOVA were used for comparison of repeated measurements within the same group (e.g. response to increasing pacing frequency). $P<0.05$ was regarded as statistically significant.

3. Results

3.1. FN increased force development in ventricular papillary muscle

Figure 1A shows that FN increased active force in a concentration-dependent manner (1 to 200 nM, n=9) at 5 Hz at 37 °C. A fit of the Boltzmann equation to the data in Fig. 1A shows that a half-maximum effect was evoked by 36.5 nM FN. Figure 1B shows typical force curves before and after application of 35.0 nM FN to a papillary muscle fiber. The peak force was enhanced by 31% after FN addition (Figure 1B). Application of FN led to an enhancement of normalized peak force as early as 1 min at 5 Hz. This enhancement peaked at 3 – 4 min (about 130 to 140% of control), remained stable for 10 min, and then declined gradually by 14–15 min (Figure 1C). Active force that describes the difference between the maximum and minimum force (passive tension) developed by the ventricle fibers increased at all given stimulation rates after application of FN (Figure 1D). The enhanced active force varied from 17% at 9 Hz to 55% at 2 Hz ($p < 0.05$, n=9). Note that the fibers also demonstrated a positive force–frequency response (FFR) from 2 to 9 Hz, similar to previous

reports [32]. BSA in the perfusion solution was used as a control, and had no significant effect on the time course of force generation (Figure 1C).

The rates of force generation and relaxation (+d*F*/d*t* and −d*F*/d*t*) were calculated as described in Methods. FN caused a significant increased in both +d*F*/d*t* and − d*F*/d*t* at all the tested stimulation frequencies between 1 and 9 Hz, ($p < 0.05$, n=9) in papillary muscle (Figures 2A and 2C). The rate of force generation increased from 18% at 9 Hz to 105% at 2 Hz (Figure 2A). Furthermore, TPF was significantly decreased in papillary fibers stimulated at all frequencies except 9 Hz after treatment with FN (Figure 2B). The rate of force relaxation increased from 23% at 9 Hz to 136% at 2 Hz (Figure 2C). The times to 50% relaxation from the peak force were 20%, 22% and 15% shorter at 1, 2 and 5 Hz, respectively, after application of FN (Figure 2D, $p < 0.05$, n = 9).

3.2. Increased force generation in FN-treated ventricular papillary fibers associated with increase in both $[Ca^{2+}]_i$ and Ca^{2+} sensitivity

To further elucidate the mechanisms for the enhancement of force in the presence of FN, we measured the force and $[Ca^{2+}]_i$ simultaneously in papillary muscle fibers at room temperature. The Ca^{2+} transients and force measured at 1 Hz before and after FN incubation are shown in Figures 3A and 3B, respectively. Both force and $[Ca^{2+}]_i$ transients were increased in the presence of FN. The Ca^{2+} transients declined faster to 50% of the peak in the presence of FN at 1 Hz (175 ± 11 ms at control *vs* 144 ± 12 ms at FN, $p < 0.05$; n=9). The relaxation time (50% from the peak) was 16% faster after application of FN. The time to peak of $[Ca^{2+}]_i$ (Figure 3A) and TPF (Figure 3B) were not significantly changed in the presence of FN. However, the time between peak Ca^{2+} and peak force was 9% shorter at 1 Hz in papillary fibers perfused with FN (Control: 85 ± 3 ms *vs* FN: 77 ± 4 ms, $p < 0.05$; n=9).

Figure 4A shows typical force - $[Ca^{2+}]_i$ loops for papillary fibers before and after FN application at 1 Hz. Note three distinct points labeled as '*A*', '*B*' and '*C*' on the force-$[Ca^{2+}]_i$ hysteresis loop. Point '*A*' represents the resting (basal) point, point '*B*' represents maximal $[Ca^{2+}]_i$ concentration and point '*C*' represents maximal force. At point '*A*', an increase in stimulation frequency did not significantly change the $[Ca^{2+}]_i$ and diastolic force of the fiber in either the control or FN-treated condition. Figures 4B and 4C show the changes in the maximum active force, maximum $[Ca^{2+}]_i$, and delta gain (DG) of active force divided by the change in $[Ca^{2+}]_i$ (active force/$\Delta[Ca^{2+}]_i$) for stimulation frequencies 1.0 Hz and 2.0 Hz that occur at point '*B*' and point '*C*', respectively. The delta gain (DG) of the active force/ $\Delta[Ca^{2+}]_i$ is defined as the active force divided by the difference in $[Ca^{2+}]_i$ from point '*B*' to point '*A*' or from point '*C*' to point '*A*'. Since delta gain quantifies changes in force per unit Ca^{2+}, the alteration in this parameter could represent changes in the myofilament activation processes [2, 31, 32], such as an increase in Ca^{2+} sensitivity. The results demonstrate that at point '*B*' (Figure 4B), the active force significantly increased by 73% and 22% at 1 Hz and 2 Hz, while the maximum Ca^{2+} was increased by 33% and 11% respectively. Furthermore, DG significantly increased by 22% at 1 Hz. At point '*C*' (Figure 4C) the maximum active force was increased by 57% and 31% at 1 Hz and 2 Hz, respectively, in the presence of FN. The $[Ca^{2+}]_i$ concentration was also increased by 26% at 1 Hz and by 12% at 2 Hz after FN application. The DG at point '*C*' significantly increased by 24% and 15% at 1.0 and 2.0 Hz, respectively, in the presence of FN.

3.3. The increased force generation in FN-treated muscle fiber is mediated by α5β1 integrins

To investigate the role of integrins in the activation effect on force development in FN-treated fibers, we pretreated the papillary fiber bundles with function blocking antibodies for

α3 or α5 integrin subunits and measured the force development as described in Methods. α3 and α5 integrin subunits are known to associate only with β1 integrin subunit, making α3 and α5 antibodies specific for α3β1 and α5β1 heterodimer integrins, respectively. The results show that the effect of FN on force was significantly attenuated in the presence of antibodies for α5 integrins (Figure 5A). The data show that the maximum force development of papillary muscle preparations was significantly reduced by 39% at 1 Hz and 36% at 2 Hz ($n=7$, $P < 0.05$) in the presence of α5 blocking antibody (α5 + FN group) compared to FN-treated fibers alone. Furthermore, the peak $[Ca^{2+}]_i$ was significantly decreased by 19% at 1 Hz in fibers treated with α5 blocking antibody compared to FN-treated fibers alone ($n=7$, $p < 0.05$). There were no significant differences in normalized peak force and $[Ca^{2+}]_i$ between control and α5 + FN groups. The effects of FN on force and $[Ca^{2+}]_i$ were not significantly affected in the presence of α3 integrin function-blocking antibody (Figure 5).

3.4. Enhanced force and Ca^{2+} by FN are PKA and L-type Ca^{2+} channel dependent

Phosphorylation via PKA at serine 1928 of the L-type Ca^{2+} channels and PKA-dependent phosphorylation of myofilament proteins and Ca^{2+}-handling proteins lead to positive inotropic, lusitropic, and chronotropic effects on the heart [38–41]. Since FN enhanced force development and increased $[Ca^{2+}]_i$ with shorter time to the peak of force development in papillary fibers, we propose that activation of both the L-type Ca^{2+} channel and PKA would be involved in modulating the $[Ca^{2+}]_i$ and myofilament or Ca^{2+}-handling proteins. To test this hypothesis, papillary muscle fibers were pretreated with the cell permeable PKA inhibitor 14–22 amide (PKA-I, 1 μM) or with the Ca^{2+} channel blocker verapamil (2.5 μM) prior to perfusion with FN. Figures 6A and 6B clearly demonstrate that the effect of FN on force development and $[Ca^{2+}]_i$ were greatly reduced in the fibers treated with PKA-I at both 1 Hz and 2 Hz. Furthermore the increase in active force per unit Ca^{2+} associated with FN treatment was significantly reduced in fibers treated with PKA-I (Table 1).

As shown in Figures 6C and 6D, verapamil significantly reduced maximum force generation by 74 and 76% at 1 and 2 Hz stimulation, respectively, while the maximum $[Ca^{2+}]_i$ was inhibited by 64 and 68% at 1 and 2 Hz, respectively. There was no further increase in active force and $[Ca^{2+}]_i$ after FN application in the presence of verapamil (Figures 6C and D).

3.5. FN enhanced myocyte cell shortening and I_{Ca}

To determine the effects of FN on the shortening of single cardiomyocytes, freshly isolated adult mouse cardiomyocytes were treated with 35 nM FN under 1 Hz field stimulation. Prior to stimulation, cell length was not significantly different in the presence of 35 nM FN (98.8 ± 4.6 μm in control vs 95.4 ± 4.7 μm after FN). Figure 7A shows typical contractions (normalized to control length) in cardiomyocytes before and after FN by 1 Hz field stimulation. Pooled average data (Figure 7B) revealed that the amplitude of contraction was increased by 40% in the presence of FN ($P<0.05$, $n=13$). The time to the peak of contraction and time to 50% relaxation were also shortened by 12% and 19%, respectively, after FN application (Figure 7C). In addition, the rates of contraction and relaxation were increased by 59% and 70%, respectively, in the presence of FN (Figure 7D).

Since force enhancement by papillary muscle was accompanied by an increase in the $[Ca^{2+}]_i$ in the presence of FN, and Ca^{2+} entry through the L-type Ca^{2+} channel is the first step leading to an $[Ca^{2+}]_i$ increase, the activity of Ca_L was examined. Whole-cell inward I_{Ca} in freshly isolated mouse cardiomyocytes was elicited by voltage steps (−60 to +40 mV in 10 mV increments, duration = 200 ms from a holding potential = −50 mV) or by voltage ramps (−50 to + 40 mV, duration = 200 ms. Figure 8A). Both protocols evoked inward currents that peaked at −10 mV and were blocked by the cardiac Ca^{2+} channel blocker verapamil (2.5 μM, Figure 8A). Application of FN (35 nM) in the bath solution led to an enhancement

of I_{Ca} (Figure 8A). Furthermore, the increase in I_{ca} was detected as early as 1 min, reached a peak at 3 to 5 min, and was followed by a gradual return (data not shown). The average response of 4 cells to FN is summarized in Figure 8B. On average, 4 min application of 35 nM FN was associated with a 36% enhancement of I_{Ca} at −10 mV. The data in Figure 8B represent the peak I_{Ca} normalized to the peak I_{Ca} recorded in the same cell just before FN application.

3.6. Phosphorylation of PLB increased in the presence of FN

To test if integrin engagement with FN led to protein phosphorylation of cardiac TnI (Ser 23/24) and phospholamban (PLB) Ser16, papillary muscles were stimulated at 3 Hz for 4 min after FN and then subjected to western blot analyses with specific antibodies. Quantitative analyses (Figure 9A) from the sample preparations either by boiling or heating to 37 °C showed that the p-PLB/total PLB ratio was significantly increased in the fibers treated with FN (Boiled samples: 0.611 ± 0.049 in FN treated vs 0.305 ± 0.061 in control; samples heated to 37 °C: 0.691 ± 0.005 in FN treated vs 0.242 ± 0.069 in control. $p < 0.05$). Analysis of p-PLB was also carried out with respect to GAPDH expression in the same samples. The ratio of p-PLB/GAPDH was significantly increased in FN-treated fibers (Boiled samples: 0.636 ± 0.044 in FN treated vs 0.358 ± 0.066 in controls; samples heated to 37 °C: 0.759 ± 0.029 in FN treated vs 0.297 ± 0.079 in controls. $p < 0.05$). As shown in Figure 9B, the p-TnI/total TnI ratio did not show any significant difference between control and FN-treated fiber samples (0.706 ± 0.039 in FN treated vs 0.732 ± 0.0125 in controls).

4. Discussion

The main goal of this study was to determine the mechanisms whereby FN modulates cardiac muscle contractility. A significant enhancement in ventricular myocyte force was recorded in the presence of FN. The increase in force was accompanied by an increase in Ca^{2+} concentration, an increase in Ca^{2+} sensitivity as deduced from analysis of Ca^{2+}-force loops, and an enhancement in the phosphorylation of phospholamban. Electrophysiological recordings of current through the L-type Ca^{2+} channel revealed an increase in I_{Ca} in the presence of FN. The enhancement of myocyte force induced by FN was significantly reversed in the presence of a function-blocking antibody against α5β1 integrin. A PKA inhibitor and a Ca^{2+} channel blocker reversed the effects of FN on muscle fiber force development. These results demonstrate that FN acts via α5β1 integrin to increase ventricular myocyte force production and that the underlying mechanisms involve an increase in $[Ca^{2+}]_i$ through the L-type Ca^{2+} channel and an increase in Ca^{2+} handling by phosphorylation of phospholamban in addition to changes in myofilament activation processes such as Ca^{2+} sensitivity and crossbridge activation in the myocardium.

4.1. FN and cardiac function

In adult myocardial tissue, the increased expression of cellular FN mRNA was seen as a response to hypertrophy that accompanied by re-expression of fetal isoforms of FN [42,43]. Moreover, accumulation of FN is observed in ischemic myocardium during the early stages of acute myocardial infarction, and may play a role in the repair process and fibrotic remodeling of the ventricular wall [44,45]. During the progression of diabetes, hypertension and myocardial infarction, there is an increase in expression and deposition of insoluble FN and collagen in non-cardiovascular myocyte compartments, which have a relatively similar distribution throughout the myocardium [46]. An imbalance in the production and the degradation of ECM proteins may lead to structural alterations such as basement membrane thickening and ECM protein deposition in tissues during the development of cardiovascular diseases [22,26,42,47–59]. All of these studies imply that FN is a major component of the myocardial interstitium, may affect myocardial compliance, and modulate the contraction

and/or relaxation cardiomyocytes. However, the role that FN plays in modulating cardiac muscle contraction has not been directly studied.

The FN polypeptide is composed of three repeat regions, I, II, and III [7,60]. The recognition site for α3β1 or α5β1 integrin is in FN region III, which contains RGD repeats. When FN binds to the integrin receptor, integrin clustering and assembly of multiple focal proteins occurs inside the cell initiating various signaling pathways. We previously showed that soluble RGD-containing synthetic peptide, or fragments of denatured collagen (Type I) significantly reduced force production in papillary muscle fibers. Integrin antibodies for α5 and β1 integrins, but not α3 integrin antibody, reversed the effect of the RGD-containing peptide. Force–$[Ca^{2+}]_i$ measurements showed that the depressed force generation in the presence of RGD peptide, acting via α5β1 integrin, was associated with reduced $[Ca^{2+}]_i$ and myofilament activation processes [2]. The data presented in this study demonstrated that soluble intact FN, acting through α5β1 integrin, enhanced force and increased $[Ca^{2+}]_i$, which might be related to activation of Ca_L and myofilament activation processes. The different downstream effects of ECM proteins through various integrins or the activation of integrins by different integrin antibodies (i.e. soluble or insoluble form) leading to specific signaling have also been reported in other studies. In VSM, soluble RGD, vitronectin, RGD containing FN fragment, as well as insoluble vitronectin inhibited Ca^{2+} current probably through αvβ3 integrin. In contrast, insoluble FN acted through α5β1 to enhance Ca^{2+} current and Ca^{2+} entry. A peptide containing the LDV sequence (in the IIICS region of FN) enhanced contraction and Ca^{2+} current through α4β1 integrin [12–14]. Soluble α5β1 antibody had no effect on Ca^{2+} currents in VSM but increased Ca^{2+} in heterologously expressed neuronal and smooth muscle Ca_L channel isoforms in HEK-293 cells [12–14]. Rueckschloss et al [23] have reported that soluble FN enhanced Ca^{2+} current in cardiomyocytes while soluble RGD peptide did not have any effect on Ca^{2+} current. Lamberts et al used a specific type 1 collagenase enzyme and observed an increase in diastolic and developed tension [61]. Laminin binding to β1 integrins modulates Ca_L through signaling pathways linked to adrenergic and cholinergic receptors signaling in cat atrial myocytes [62,63]. The difference in the downstream signaling observed between RGD-containing collagen and FN could be explained by the activation of different intracellular signaling pathways. Digested/soluble collagen, upon binding to α5β1 integrin, activated protein kinase C to inhibit Ca_L and decreased Ca^{2+} to myofilaments [2]; whereas in this study we showed that binding of intact soluble FN to α5β1 integrin activated PKA and increased phosphorylation of PLB and thereby enhanced Ca^{2+} sensitivity and crossbridge kinetics. Thus, it is likely that the overlapping distribution of FN and collagen in the myocardial matrix that have differential functions on cardiomyocytes whose actions might represent an equilibrium mechanism during physiological or pathological circumstances.

4.2. FN modulates cardiac contractility through Ca^{2+} signaling, Ca^{2+} sensitivity and crossbridge kinetics

The data presented in figures 1 and 4 clearly show an increase in force development in the FN-treated fibers. Though the active force (total force – passive force) values at 1.0 Hz are comparable both at room temperature and 37°C (for control samples: 10.7 ± 1.2 mN/mm2 at room temperature and 11.8 ± 1.8 at 37°C; the values are from data shown in figure 1D and figure 4C, respectively), the force values are higher in the fibers stimulated at 2.0 Hz measured at room temperature. We think the force values are different due to the temperature at which the experiments have been performed. These data are also consistent with our previous publication [32], which showed that the maximum force at 34°C peaks at 6–7 Hz, whereas at room temperature the force peaks at 3.0 Hz. The simultaneous force and

Ca^{2+} measurements were performed at room temperature, since Fura-2 dye load into myocytes more efficiently at room temperature as we have discussed in the Methods section.

The level of $[Ca^{2+}]_i$ along with the sensitivity of the myofilaments to $[Ca^{2+}]_i$, determine the level of activation of the cardiac muscle fibers. Increasing stimulation frequency caused a progressive an increase in myocyte force development, which is evident as a positive force-frequency relationship (FFR) in both control and FN-treated groups. Several studies have shown that the Ca_L channel and the Ca^{2+} handling protein sarcoplasmic reticulum Ca^{2+} ATPase (SERCA2a) have frequency-dependent characteristics that contribute to a positive FFR [64–67]. Phosphorylation of the PKA site on the Ca_L channel causes an increase in the open probability and the open time, leading to an increased influx of Ca^{2+} and enhancement of cardiac excitation-contraction due to an increase in the free cytosolic Ca^{2+} concentration [68–70]. As evident from the presented data, the increased force, $[Ca^{2+}]_i$ and I_{Ca} stimulated by FN were significantly inhibited by verapamil and PKA-I, suggesting that the FN affected force generation in cardiomyocyte through activation of Ca_L and increase in PKA activity. Ca^{2+} release and Ca^{2+} reload are also involved in the regulation of free $[Ca^{2+}]_i$, which was supported by an increase in the phosphorylation of PLB In this study, faster declined time of Ca^{2+} transients to 50% of the peak $[Ca^{2+}]_i$ during relaxation (Figure 3), indicating faster Ca^{2+} reload by FN. Additional experiments are warranted to directly test the SERCA2a activity.

Increases in $[Ca^{2+}]_i$, force and force/unit Ca^{2+} in the FN-treated papillary fibers at the point of the Ca^{2+} peak (Point '*B*') point to Ca^{2+}-activated thin filament activation processes, such as an increase in Ca^{2+} sensitivity, during the *A* to *B* segment of the force-Ca^{2+} loop. The *B* to *C* segment is typically attributed to strongly-bound crossbridges keeping tropomyosin in the open state to allow continued myosin attachment to actin despite decreasing $[Ca^{2+}]_i$ [32]. Increased force and force/unit Ca^{2+} at the point of maximum force ('*C*') suggest an increased rate of contraction and decreased time of peak Ca^{2+} to peak force; these processes may reflect an increased cooperative feedback effect and accelerated cross-bridge kinetics in the presence of FN. Furthermore, despite a small increase in $[Ca^{2+}]_i$, both at *B* and *C* points, the effect of FN on the force development is relatively greater (Figure 4), which strongly demonstrate an increase in myofilament Ca^{2+} sensitivity in the FN-treated myocardium. In addition, FN enhanced papillary muscle twitch force, cell contraction speed, and Ca^{2+} transient decay, suggesting an enhancement in Ca^{2+} dynamics, which would also augment the faster crossbridge kinetics.

4.3. Role of PKA in the downstream effects of FN-integrin adhesion

PKA activation has been shown to be involved in multiple signaling pathways downstream from integrin-ECM interactions. In migrating cells, the participation of α4β1 or α5β1 integrins in adhesion-mediated, and localized activation of PKA is one of the earliest steps in directional cell migration [71]. Several studies in myocardium have shown that PKA-dependent phosphorylation of both Ca^{2+} handling (SERCA2a, PLB, ryanodine receptor and Ca_L) and myofilament (TnI and myosin binding protein-C) proteins play a critical role in modulating the crossbridge kinetics [72–74]; however adhesion-mediated activation of PKA in the myocardium has not been previously shown. Our results, showing reversal of the FN-stimulatory effect on force development of papillary muscle fibers by PKA-I indicate that PKA is acting downstream of the FN–integrin axis to modulate the force generation in the myocardium. The presented data (Table 1), demonstrating a significant decrease in FN-augmented force per unit Ca^{2+} in the presence of PKA-I at both points B and C in the force-Ca^{2+} loop suggest that both Ca^{2+} activation of the thin filament (*A* to *B* segment) and positive feedback by strongly-bound crossbridge mechanisms (*B* to *C* segment [31,32]), are to a large extent mediated by PKA in FN-treated myofibers. Furthermore, western blotting data showed an increase in the phosphorylation of PLB. Increased phosphorylation of PLB

has been reported during catecholamine stimulation and β-adrenergic-induced acceleration of cardiac relaxation [29,75]. Taken together, our data indicate that in the presence of FN, α5β1 integrin-mediated signaling changes the characteristics of Ca^{2+}-handling protein, PLB, through PKA, which further alters the myofilament activation processes, such as Ca^{2+} sensitivity and crossbridge activation, leading to the observed enhancement of force. Cheng et al [76] have demonstrated that the overexpression of β1A integrin subunit decreases the isoproterenol-induced Ca^{2+} current and also, decreases the levels of cAMP. A different downstream effect of β1 integrin activation seen by Cheng et al [76] could be due to the fact that in our study we used FN that only binds to α5β1 or α3β1; where as, in Cheng et al overexpression of the β1A integrin subunit that would associate primarily with α1, α3, α5 and α6 integrin subunits in cardiomyocytes showed a decrease PKA activation.

This study identifies an important role for the FN–α5β1 integrin signaling pathway in cardiac myocytes relative to myocyte contractile function. The data presented here provide the first experimental evidence that FN enhances force in mouse papillary muscle fibers through α5β1 integrins. We speculate that this increase in force by FN would probably temporarily compensate for impaired heart function from overload in the hypertrophied or damaged heart. Furthermore the augmentation of force in the presence of FN is associated with an increase in $[Ca^{2+}]_i$ and changes in the myofilament activation processes, partially due to the effects of PKA on PLB. These data, along with our previous study showing that digested collagen fragments or RGD containing peptide decrease cardiomyocyte force [2], indicate that the dynamic adhesion events between ECM proteins and integrins, which are dramatically altered during the development of disease conditions in myocardium, play significant roles in modulating cardiac muscle dynamics. We have recently shown [3] that FN-integrin adhesion force and adhesion probability in contracted cells are greater than in cells under relaxed condition. We propose that the continuing alterations in integrin adhesion to the ECM would initiate outside in signaling changes that includes the changes/activation in the costamere complex and its associated kinases, to provide feedback responses of the contractile status of the cells. Our data presented in this study showed that FN-induces a Ca^{2+} increase and an increase in force development in mouse papillary muscle fibers as a feedback response to FN- α5β1 integrin interaction. However, further experiments are warranted to address how the pathological remodeling of ECM proteins including increase levels of FN affects the outside in signaling pathways in modulating the cardiac muscle contractility.

Acknowledgments

This work was supported by National Institutes of Health grants R21-EB-003888-01A1 and KO2HL-86650.

REFERENCES

1. Epstein ND, Davis JS. Sensing stretch is fundamental. Cell 2003 Jan 24;112(2):147–150. [PubMed: 12553903]
2. Sarin V, Gaffin RD, Meininger GA, Muthuchamy M. Arginine-glycine-aspartic acid (RGD)-containing peptides inhibit the force production of mouse papillary muscle bundles via alpha 5 beta 1 integrin. J Physiol 2005 Apr 15;564(Pt 2):603–617. [PubMed: 15718258]
3. Wu X, Sun Z, Foskett A, Trzeciakowski JP, Meininger GA, Muthuchamy M. Cardiomyocyte contractile status is associated with differences in fibronectin and integrin interactions. Am J Physiol Heart Circ Physiol 2010 Jun;298(6):H2071–H2081. [PubMed: 20382852]
4. Ross RS, Borg TK. Integrins and the myocardium. Circ Res 2001;88(11):1112–1119. [PubMed: 11397776]
5. Samarel AM. Costameres, focal adhesions, and cardiomyocyte mechanotransduction. Am J Physiol Heart Circ Physiol 2005 Dec;289(6):H2291–H2301. [PubMed: 16284104]

6. Glukhova, M.; Koteliansky, V. Integrins, cytoskeletal,extracellular matrix proteins in developing smooth muscle cells of human aorta. In: Schwartz, S.; Mecham, R., editors. The Vascular Smooth Muscle Cell: Molecular and Biological Responses to the Extracellular Matrix. San Diego, CA: Academic Press; 1995. p. 37-79.
7. Jane-Lise S, Corda S, Chassagne C, Rappaport L. The extracellular matrix and the cytoskeleton in heart hypertrophy and failure. Heart Fail Rev 2000 Oct;5(3):239–250. [PubMed: 16228907]
8. Wang N, Butler JP, Ingber DE. Mechanotransduction across the cell surface and through the cytoskeleton. Science 1993;260:1124–1127. [PubMed: 7684161]
9. McNamee HP, Ingber DE, Schwartz MA. Adhesion to fibronectin stimulates inositol lipid synthesis and enhances PDGF-induced inositol lipid breakdown. J Cell Biol 1993 May;121(3):673–678. [PubMed: 8387531]
10. Schmidt C, Pommerenke H, Durr F, Nebe B, Rychly J. Mechanical stressing of integrin receptors induces enhanced tyrosine phosphorylation of cytoskeletally anchored protein. The Journal of Biological Chemistry 1998;273:5081–5085. [PubMed: 9478959]
11. Wu X, Davis GE, Meininger GA, Wilson E, Davis MJ. Regulation of the L-type calcium channel by alpha 5beta 1 integrin requires signaling between focal adhesion proteins. J Biol Chem 2001;276(32):30285–30292. [PubMed: 11382763]
12. Wu X, Mogford JE, Platts SH, Davis GE, Meininger GA, Davis MJ. Modulation of calcium current in arteriolar smooth muscle by alphav beta3 and alpha5 beta1 integrin ligands. J Cell Biol 1998;143(1):241–252. [PubMed: 9763435]
13. Waitkus-Edwards KR, Martinez-Lemus LA, Wu X, Trzeciakowski JP, Davis MJ, Davis GE, et al. alpha(4)beta(1) Integrin activation of L-type calcium channels in vascular smooth muscle causes arteriole vasoconstriction. Circ Res 2002;90(4):473–480. [PubMed: 11884378]
14. Gui P, Wu X, Ling S, Stotz SC, Winkfein RJ, Wilson E, et al. Integrin receptor activation triggers converging regulation of Cav1.2 calcium channels by c-Src and protein kinase A pathways. J Biol Chem 2006 May 19;281(20):14015–14025. [PubMed: 16554304]
15. Gui, P.; Balasubramanian, B.; Wu, X.; Ling, S.; Stotz, S.; Wilson, E., et al. Effect of α5β1 Integrin Activation on Heterologously Expressed Cardiac L-type Calcium Channels (abstract); 48th Annual Meeting of Biophysical Society; Baltimore: 2004. 2004. p. **
16. Wu X, Yang Y, Gui P, Sohma Y, Meininger GA, Davis GE, et al. Potentiation of large conductance, Ca2+-activated K+ (BK) channels by alpha5beta1 integrin activation in arteriolar smooth muscle. J Physiol 2008 Mar 15;586(6):1699–1713. [PubMed: 18218680]
17. Yang Y, Wu X, Gui P, Wu J, Sheng JZ, Ling S, et al. Alpha5beta1 integrin engagement increases large conductance, Ca2+-activated K+ channel current and Ca2+ sensitivity through c-src-mediated channel phosphorylation. J Biol Chem 2010 Jan 1;285(1):131–141. [PubMed: 19887442]
18. Passier R, Zeng H, Frey N, Naya FJ, Nicol RL, McKinsey TA, et al. CaM kinase signaling induces cardiac hypertrophy and activates the MEF2 transcription factor in vivo. J Clin Invest 2000 May; 105(10):1395–1406. [PubMed: 10811847]
19. Sei CA, Irons CE, Sprenkle AB, McDonough PM, Brown JH, Glembotski CC. The alpha-adrenergic stimulation of atrial natriuretic factor expression in cardiac myocytes requires calcium influx, protein kinase C, and calmodulin-regulated pathways. J Biol Chem 1991 Aug 25;266(24): 15910–15916. [PubMed: 1714900]
20. Clark RJ, McDonough PM, Swanson E, Trost SU, Suzuki M, Fukuda M, et al. Diabetes and the accompanying hyperglycemia impairs cardiomyocyte calcium cycling through increased nuclear O-GlcNAcylation. J Biol Chem 2003 Nov 7;278(45):44230–44237. [PubMed: 12941958]
21. Belke DD, Swanson EA, Dillmann WH. Decreased sarcoplasmic reticulum activity and contractility in diabetic db/db mouse heart. Diabetes 2004 Dec;53(12):3201–3208. [PubMed: 15561951]
22. Belke DD, Dillmann WH. Altered cardiac calcium handling in diabetes. Curr Hypertens Rep 2004 Dec;6(6):424–429. [PubMed: 15527685]
23. Rueckschloss U, Isenberg G. Contraction augments L-type Ca2+ currents in adherent guinea-pig cardiomyocytes. J Physiol 2004 Oct 15;560(Pt 2):403–411. [PubMed: 15297568]

24. Trial J, Rossen RD, Rubio J, Knowlton AA. Inflammation and ischemia: macrophages activated by fibronectin fragments enhance the survival of injured cardiac myocytes. Exp Biol Med (Maywood) 2004 Jun;229(6):538–545. [PubMed: 15169973]
25. Chen H, Huang XN, Stewart AF, Sepulveda JL. Gene expression changes associated with fibronectin-induced cardiac myocyte hypertrophy. Physiol Genomics 2004 Aug 11;18(3):273–283. [PubMed: 15306692]
26. Mamuya WS, Brecher P. Fibronectin expression in the normal and hypertrophic rat heart. J Clin Invest 1992 Feb;89(2):392–401. [PubMed: 1531344]
27. Ahumada GG, Saffitz JE. Fibronectin in rat heart: a link between cardiac myocytes and collagen. J Histochem Cytochem 1984 Apr;32(4):383–388. [PubMed: 6707462]
28. Laser M, Willey CD, Jiang W, Cooper Gt, Menick DR, Zile MR, et al. Integrin activation and focal complex formation in cardiac hypertrophy. J Biol Chem 2000 Nov 10;275(45):35624–35630. [PubMed: 10958798]
29. Li L, Desantiago J, Chu G, Kranias EG, Bers DM. Phosphorylation of phospholamban and troponin I in beta-adrenergic-induced acceleration of cardiac relaxation. Am J Physiol Heart Circ Physiol 2000 Mar;278(3):H769–H779. [PubMed: 10710345]
30. Grynkiewicz G, Poenie M, Tsien R. A new generation of Ca2+ indicators with greatly improved fluorescence properties. The Journal of Biological Chemistry 1985;260:3440–3450. [PubMed: 3838314]
31. Gaffin RD, Tong CW, Zawieja DC, Hewett TE, Klevitsky R, Robbins J, et al. Charged residue alterations in the inner-core domain and carboxy-terminus of alpha-tropomyosin differentially affect mouse cardiac muscle contractility. J Physiol 2004 Dec 15;561(Pt 3):777–791. [PubMed: 15486021]
32. Tong CW, Gaffin RD, Zawieja DC, Muthuchamy M. Roles of phosphorylation of myosin binding protein-C and troponin I in mouse cardiac muscle twitch dynamics. J Physiol 2004 Aug 1;558(Pt 3):927–941. [PubMed: 15194741]
33. Hamill OP, Marty A, Neher E, Sakmann B, Sigworth FJ. Improved patch-clamp techniques for high-resolution current recording from cells and cell-free membrane patches. Pflugers Arch 1981 Aug;391(2):85–100. [PubMed: 6270629]
34. Davis MJ. An improved, computer-based method to automatically track internal and external diameter of isolated microvessels. Microcirculation 2005 Jun;12(4):361–372. [PubMed: 16020082]
35. Dias FA, Walker LA, Arteaga GM, Walker JS, Vijayan K, Pena JR, et al. The effect of myosin regulatory light chain phosphorylation on the frequency-dependent regulation of cardiac function. J Mol Cell Cardiol 2006 Aug;41(2):330–339. [PubMed: 16806259]
36. Kolwicz SC, Kubo H, MacDonnell SM, Houser SR, Libonati JR. Effects of forskolin on inotropic performance and phospholamban phosphorylation in exercise-trained hypertensive myocardium. J Appl Physiol 2007 Feb;102(2):628–633. [PubMed: 17082376]
37. Chen W, Lah M, Robinson PJ, Kemp BE. Phosphorylation of phospholamban in aortic smooth muscle cells and heart by calcium/calmodulin-dependent protein kinase II. Cell Signal 1994 Aug; 6(6):617–630. [PubMed: 7857766]
38. Striessnig J. Pharmacology, structure and function of cardiac L-type Ca(2+) channels. Cell Physiol Biochem 1999;9(4–5):242–269. [PubMed: 10575201]
39. Hulme JT, Westenbroek RE, Scheuer T, Catterall WA. Phosphorylation of serine 1928 in the distal C-terminal domain of cardiac CaV1.2 channels during beta1-adrenergic regulation. Proc Natl Acad Sci U S A 2006 Oct 31;103(44):16574–16579. [PubMed: 17053072]
40. Kentish JC, McCloskey DT, Layland J, Palmer S, Leiden JM, Martin AF, et al. Phosphorylation of troponin I by protein kinase A accelerates relaxation and crossbridge cycle kinetics in mouse ventricular muscle. Circ Res 2001 May 25;88(10):1059–1065. [PubMed: 11375276]
41. Tong CW, Stelzer JE, Greaser ML, Powers PA, Moss RL. Acceleration of crossbridge kinetics by protein kinase A phosphorylation of cardiac myosin binding protein C modulates cardiac function. Circ Res 2008 Oct 24;103(9):974–982. [PubMed: 18802026]

42. Samuel JL, Barrieux A, Dufour S, Dubus I, Contard F, Koteliansky V, et al. Accumulation of fetal fibronectin mRNAs during the development of rat cardiac hypertrophy induced by pressure overload. J Clin Invest 1991;88(5):1737–1746. [PubMed: 1834701]
43. Farhadian F, Contard F, Corbier A, Barrieux A, Rappaport L, Samuel JL. Fibronectin expression during physiological and pathological cardiac growth. J Mol Cell Cardiol 1995 Apr;27(4):981–990. [PubMed: 7563110]
44. Casscells, W.; Ferrans, VJ. Growth factors in the heart. In: Oberpriller, JO.; Oberpriller, JS.; Mauro, A., editors. The development and regenerative potential of cardiac muscle. New York: Harvard; 1990. p. 8-21.
45. Knowlton AA, Connelly CM, Romo GM, Mamuya W, Apstein CS, Brecher P. Rapid expression of fibronectin in the rabbit heart after myocardial infarction with and without reperfusion. J Clin Invest 1992 Apr;89(4):1060–1068. [PubMed: 1556175]
46. Bouzeghrane F, Reinhardt DP, Reudelhuber TL, Thibault G. Enhanced expression of fibrillin-1, a constituent of the myocardial extracellular matrix in fibrosis. Am J Physiol Heart Circ Physiol 2005 Sep;289(3):H982–H991. [PubMed: 15849235]
47. Siperstein MD, Unger RH, Madison LL. Studies of muscle capillary basement membranes in normal subjects, diabetic, and prediabetic patients. J Clin Invest 1968 Sep;47(9):1973–1999. [PubMed: 5675423]
48. Weber K. Extracellular matrix remodeling in heart failure: a role for de novo angiotensin II generation. Circulation 1997;96(11):4065–4082. [PubMed: 9403633]
49. Villarreal FJ, Dillmann WH. Cardiac hypertrophy-induced changes in mRNA levels for TGF-beta 1, fibronectin, and collagen. Am J Physiol 1992;262(6 pt 2):H1861–H1866. [PubMed: 1535758]
50. Contard F, Koteliansky V, Marotte F, Dubus I, Rappaport L, Samuel JL. Specific alterations in the distribution of extracellular matrix components within rat myocardium during the development of pressure overload. Lab Invest 1991;64(1):65–75. [PubMed: 1824954]
51. Willems IE, Arends JW, Daemen MJ. Tenascin and fibronectin expression in healing human myocardial scars. J Pathol 1996;179(3):321–325. [PubMed: 8774490]
52. Ulrich MM, Janssen AM, Daemen MJ, Rappaport L, Samuel JL, Contard F, et al. Increased expression of fibronectin isoforms after myocardial infarction in rats. J Mol Cell Cardiol 1997;29(9):2533–2543. [PubMed: 9299376]
53. McCrossan ZA, Billeter R, White E. Transmural changes in size, contractile and electrical properties of SHR left ventricular myocytes during compensated hypertrophy. Cardiovasc Res 2004 Aug 1;63(2):283–292. [PubMed: 15249186]
54. Kaur H, Chen S, Xin X, Chiu J, Khan ZA, Chakrabarti S. Diabetes-induced extracellular matrix protein expression is mediated by transcription coactivator p300. Diabetes 2006 Nov;55(11):3104–3111. [PubMed: 17065349]
55. Fredersdorf S, Thumann C, Ulucan C, Griese DP, Luchner A, Riegger GA, et al. Myocardial hypertrophy and enhanced left ventricular contractility in Zucker diabetic fatty rats. Cardiovasc Pathol 2004 Jan-Feb;13(1):11–19. [PubMed: 14761780]
56. Grimm D, Huber M, Jabusch HC, Shakibaei M, Fredersdorf S, Paul M, et al. Extracellular matrix proteins in cardiac fibroblasts derived from rat hearts with chronic pressure overload: effects of beta-receptor blockade. J Mol Cell Cardiol 2001 Mar;33(3):487–501. [PubMed: 11181017]
57. Brownlee M. The pathobiology of diabetic complications: a unifying mechanism. Diabetes 2005 Jun;54(6):1615–1625. [PubMed: 15919781]
58. Roy S, Sala R, Cagliero E, Lorenzi M. Overexpression of fibronectin induced by diabetes or high glucose: phenomenon with a memory. Proc Natl Acad Sci U S A 1990 Jan;87(1):404–408. [PubMed: 2296596]
59. Smoak IW. Hyperglycemia-induced TGFbeta and fibronectin expression in embryonic mouse heart. Dev Dyn 2004 Sep;231(1):179–189. [PubMed: 15305298]
60. Dalen H, Saetersdal T, Roli J, Larsen TH. Effect of collagenase on surface expression of immunoreactive fibronectin and laminin in freshly isolated cardiac myocytes. J Mol Cell Cardiol 1998 May;30(5):947–955. [PubMed: 9618235]

61. Lamberts RR, Willemsen MJ, Perez NG, Sipkema P, Westerhof N. Acute and specific collagen type I degradation increases diastolic and developed tension in perfused rat papillary muscle. Am J Physiol Heart Circ Physiol 2004 Mar;286(3):H889–H894. [PubMed: 14576082]
62. Wang YG, Samarel AM, Lipsius SL. Laminin binding to beta1-integrins selectively alters beta1- and beta2-adrenoceptor signalling in cat atrial myocytes. J Physiol 2000;527(Pt 1):3–9. [PubMed: 10944166]
63. Wang YG, Samarel AM, Lipsius SL. Laminin acts via beta 1 integrin signalling to alter cholinergic regulation of L-type Ca(2+) current in cat atrial myocytes. J Physiol 2000;526(Pt 1):57–68. [PubMed: 10878099]
64. Lemaire S, Piot C, Leclercq F, Leuranguer V, Nargeot J, Richard S. Heart rate as a determinant of L-type Ca2+ channel activity: mechanisms and implication in force-frequency relation. Basic Res Cardiol 1998;(93 Suppl 1):51–59. [PubMed: 9833131]
65. Alpert NR, Leavitt BJ, Ittleman FP, Hasenfuss G, Pieske B, Mulieri LA. A mechanistic analysis of the force-frequency relation in non-failing and progressively failing human myocardium. Basic Res Cardiol 1998;(93 Suppl 1):23–32. [PubMed: 9833127]
66. Hashimoto K, Perez NG, Kusuoka H, Baker DL, Periasamy M, Marban E. Frequency-dependent changes in calcium cycling and contractile activation in SERCA2a transgenic mice. Basic Res Cardiol 2000 Apr;95(2):144–151. [PubMed: 10826507]
67. Miyamoto MI, del Monte F, Schmidt U, DiSalvo TS, Kang ZB, Matsui T, et al. Adenoviral gene transfer of SERCA2a improves left-ventricular function in aortic-banded rats in transition to heart failure. Proc Natl Acad Sci U S A 2000 Jan 18;97(2):793–798. [PubMed: 10639159]
68. Hescheler J, Fleischmann BK. Regulation of voltage-dependent Ca2+ channels in the early developing heart: role of beta1 integrins. Basic Res Cardiol 2002;(97 Suppl 1):I153–I158. [PubMed: 12479249]
69. Sculptoreanu A, Rotman E, Takahashi M, Scheuer T, Catterall WA. Voltage-dependent potentiation of the activity of cardiac L-type calcium channel alpha 1 subunits due to phosphorylation by cAMP-dependent protein kinase. Proc Natl Acad Sci U S A 1993 Nov 1;90(21):10135–10139. [PubMed: 7694283]
70. Sculptoreanu A, Scheuer T, Catterall WA. Voltage-dependent potentiation of L-type Ca2+ channels due to phosphorylation by cAMP-dependent protein kinase. Nature 1993 Jul 15;364(6434):240–243. [PubMed: 8391648]
71. Lim CJ, Kain KH, Tkachenko E, Goldfinger LE, Gutierrez E, Allen MD, et al. Integrin-mediated protein kinase A activation at the leading edge of migrating cells. Mol Biol Cell 2008 Nov;19(11): 4930–4941. [PubMed: 18784251]
72. Strang KT, Sweitzer NK, Greaser ML, Moss RL. Beta-adrenergic receptor stimulation increases unloaded shortening velocity of skinned single ventricular myocytes from rats. Circ Res 1994 Mar; 74(3):542–549. [PubMed: 8118962]
73. Solaro RJ, Rarick HM. Troponin and tropomyosin: proteins that switch on and tune in the activity of cardiac myofilaments. Circ Res 1998 Sep 7;83(5):471–480. [PubMed: 9734469]
74. Winegrad S. Myosin binding protein C, a potential regulator of cardiac contractility. Circ Res 2000 Jan 7–21;86(1):6–7. [PubMed: 10625298]
75. Kranias EG, Solaro RJ. Phosphorylation of troponin I and phospholamban during catecholamine stimulation of rabbit heart. Nature 1982 Jul 8;298(5870):182–184. [PubMed: 6211626]
76. Cheng Q, Ross RS, Walsh KB. Overexpression of the integrin beta(1A) subunit and the beta(1A) cytoplasmic domain modifies the beta-adrenergic regulation of the cardiac L-type Ca(2+)current. J Mol Cell Cardiol 2004 Jun;36(6):809–819. [PubMed: 15158122]

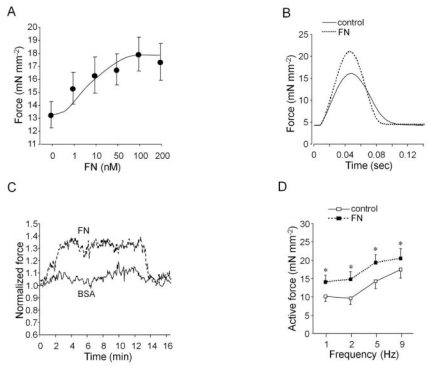

Fig. 1.

Force generation in the presence of fibronectin (FN, 35 nM) in mouse right ventricular papillary muscles. (A) FN caused a concentration-dependent increase in active force generation at 5 Hz and 37 °C. Data were fit by a Boltzmann equation with half-maximal force equal to 36.5 nM FN. (B) A typical force curve showing that force increased in the presence of FN at 5 Hz. (C) A representative trace showing the effect of FN on the active force generated by a mouse papillary muscle fiber. Bovine serum albumin (BSA, 35 nM) was used as control protein. (D) Changes of peak active force in the presence of FN at stimulation rates of 1 Hz to 9 Hz. Data are presented as mean ± SEM. n = 9. * $p < 0.05$ *vs* control.

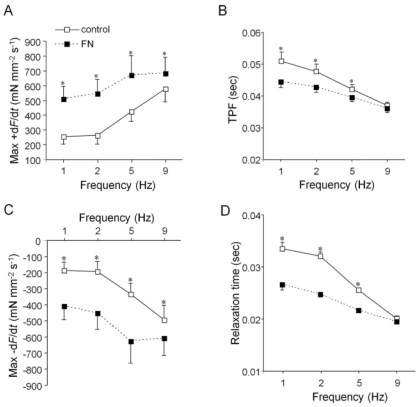

Fig. 2.

FN enhanced both the contraction and relaxation parameters in papillary muscle. (A) and (C) The maximum rates of contraction and relaxation (+d*F*/d*t* and −d*F*/d*t*) are enhanced in fibers treated with FN. (B and D) TPF and the time to 50% off the peak of maximum force are lower in the FN-treated fibers. Data are presented as mean ± SEM. n = 9; TPF: time-to-peak force. * $p < 0.05$ *vs* control.

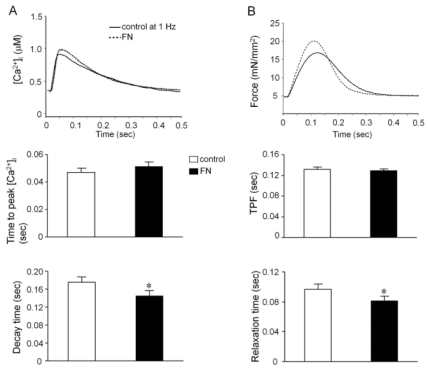

Fig. 3.

Ca^{2+} transient and force during a contraction cycle before and after FN application. Raw data showing $[Ca^{2+}]_i$ transients (A) and force (B) in top panels. Force and $[Ca^{2+}]_i$ with respect to time at a stimulation rate = 1 Hz. Decay time of $[Ca^{2+}]_i$ and force relaxation time are the times representing EC_{50} values. TPF: time-to-peak force. Data are presented as mean ± SEM. n = 9. * $p < 0.05$ *vs* control.

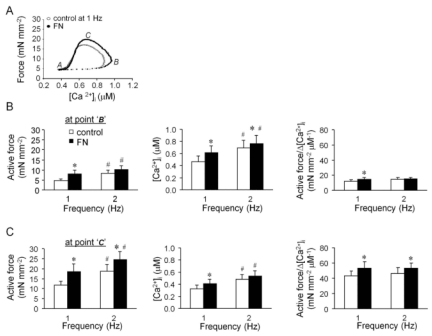

Fig. 4.

Analysis of the force-$[Ca^{2+}]_i$ loop in the absence and presence of FN. (A) Representative force- Ca^{2+} loop in the absence and presence of FN at a stimulation rate = 1 Hz. '*A*' is the resting point; '*B*' is the peak $[Ca^{2+}]_i$ point; and '*C*' is the peak force point. (B) and (C) $[Ca^{2+}]_i$, active force, and active force/$\Delta[Ca^{2+}]_i$ in the absence and presence of FN (n=9). Data are presented as mean ± SEM. * $p < 0.05$ *vs* control of corresponding rates. # $p < 0.05$ *vs* 1 Hz within control or FN group.

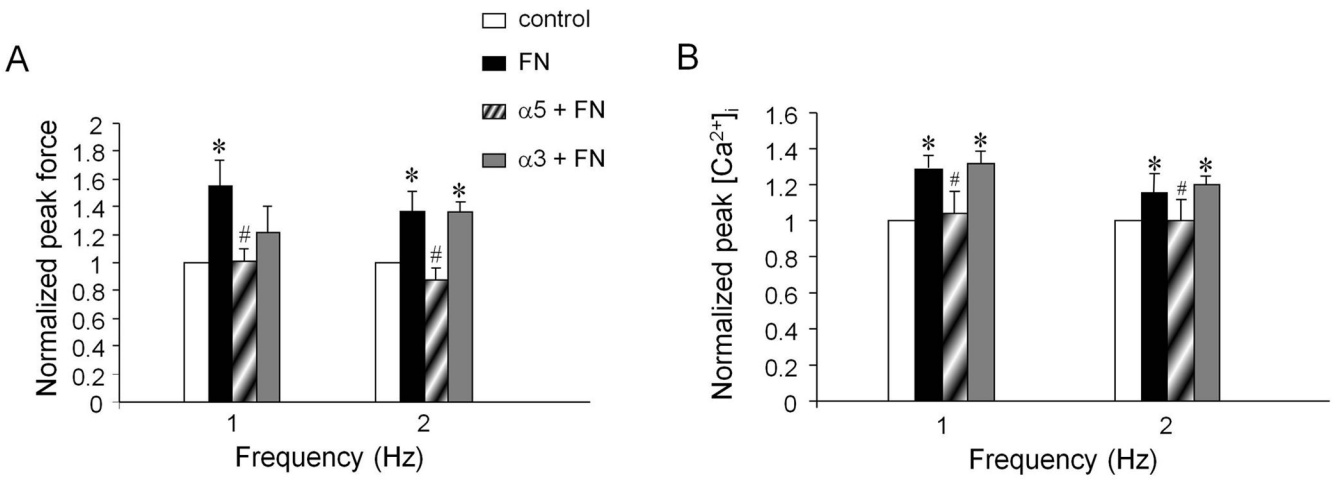

Fig. 5.

The FN-enhancement in peak force and $[Ca^{2+}]_i$ were inhibited by an α5 integrin function blocking antibody. Bar graph summary of normalized force changes (A) or $[Ca^{2+}]_i$ (B) after FN (n = 9) or after pretreatment with α3 integrin function blocking antibody (60 nM, n = 7) or α5 integrin function blocking antibody (60 nM, n = 7) at 1 or 2 Hz rate. * $p < 0.05$ *vs* control. # $p < 0.05$ *vs* FN alone.

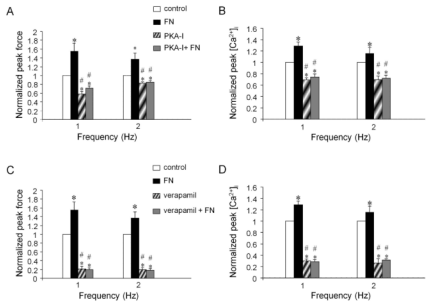

Fig. 6.

FN enhanced force and $[Ca^{2+}]_i$ were blocked by PKA inhibitor (PKA-I) or L-type Ca^{2+} channels blocker verapamil. Bar graph summary of normalized peak force changes (A or C) and peak $[Ca^{2+}]_i$ (B or D) in the pretreatment of PKA-I (1 μM, n = 6, A and B) or verapamil (2.5 μM, n = 7. C and D) at 1 or 2 Hz rate. There are no differences before and after application of FN in the presence of PKA-I or verapamil. * $p < 0.05$ *vs* control. # $p < 0.05$ *vs* FN alone.

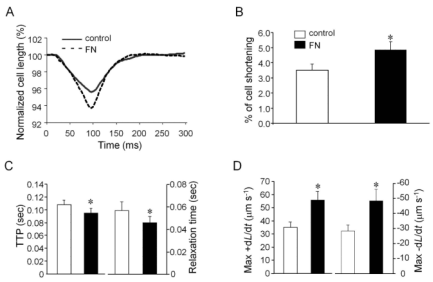

Fig. 7.

The effects of FN on cell contraction. (A) Representative tracings of cell shortening triggered by 1 Hz field stimulation before and after FN application in adult cardiomyocytes. In the presence of FN (35 nM), increased fractional shortening, shorter time to peak of shortening (TTP), and shorter time to half relaxation (relaxation time) are evident (B) and (C) (n=13). (D) Pooled data showing higher rates of contraction and relaxation in the presence of FN. * $p < 0.05$ *vs* control.

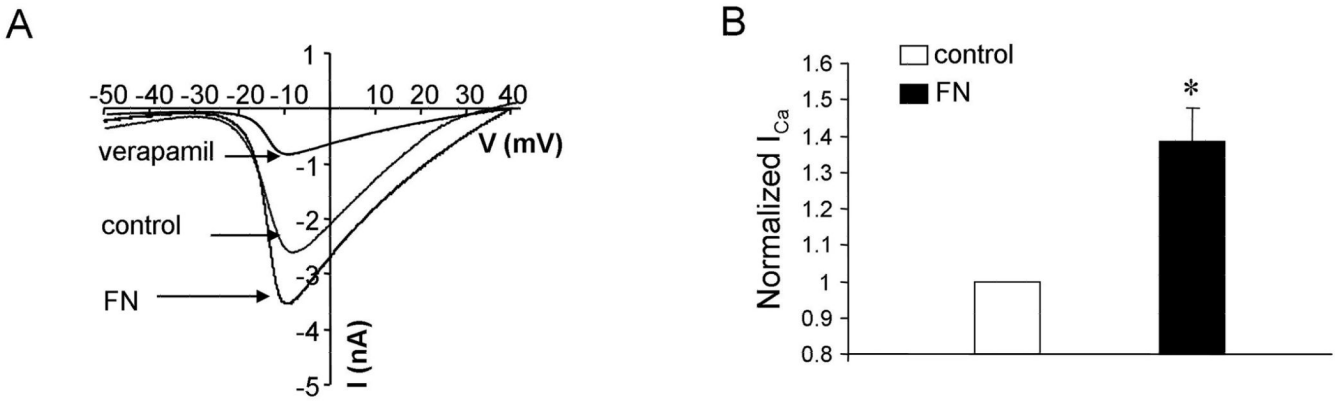

Fig. 8.

The effects of FN on L-type Ca^{2+} channel (Ca_L). (A) Whole-cell inward Ca_L currents (I_{Ca}) - voltage (I–V) relationships obtained from freshly isolated adult mouse cardiomyocyte using a ramp protocol (−50 to +40 mV over 200 ms). I_{Ca} was enhanced at 4 min after application of FN (35 nM). The current was substantially inhibited by 2.5 μM verapamil. (B) Bar graph represents normalized peak currents 4 min after application of FN, where current was significantly enhanced (n=4). Peak currents after FN were normalized to the currents at the peak of the control I–V relationship (usually at a test potential of −10 mV). * $p < 0.05$ *vs* control. Pipette: 110 Cs+; bath: 2 mM Ba^{2+}; holding potential: −50 mV.

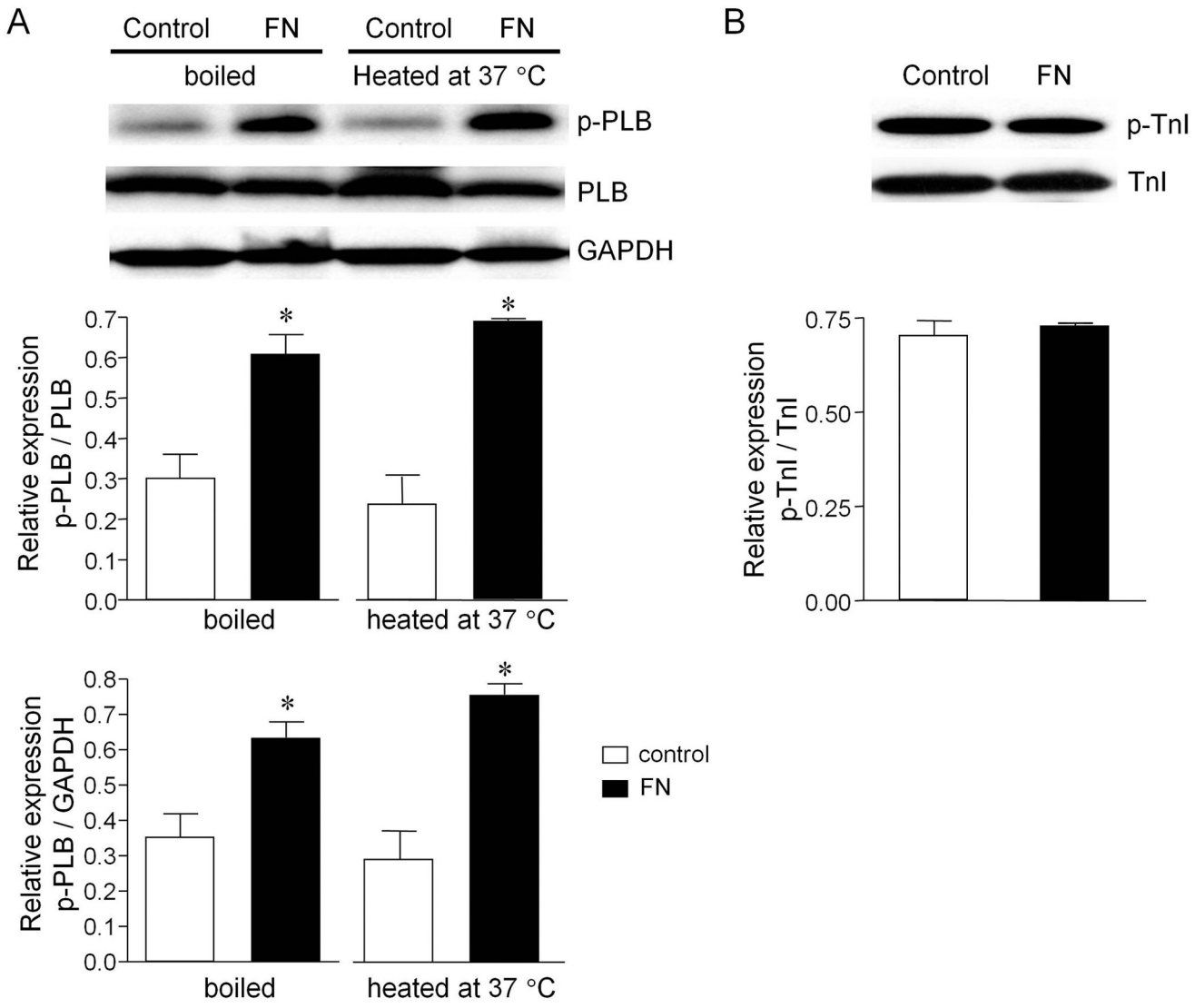

Fig. 9.

Western blot analysis of p-PLB and p-TnI expression with or without FN treatment: Mouse papillary muscle bundles were subjected to FN treatment (stimulated at 3 Hz) and analyzed for differential expression of p-PLB and p-TnI. (A) Top panel: Representative blot showing the expression of p-PLB, PLB and GAPDH in control and FN-treated samples that were boiled or heated to 37 °C. Bottom panel: The relative expression of p-PLB/PLB and p-PLB/GAPDH were calculated and plotted. (B) Top panel: Representative blot showing the expression of p-TnI and TnI in control and FN-treated samples. Bottom panel: The relative expression of p-TnI/TnI was calculated and plotted. Both A and B represent data from three independent experiments and the mean ± SEM is plotted. * $p < 0.05$ *vs* control.

Table 1

Active force per unit Ca^{2+} changes after application of FN in the presence of PKA inhibitor (PKA-I).

at 2 Hz	Control	FN (n=9)	PKA-I (n=6)	PKA-I + FN (n=6)
Active force / $\Delta[Ca^{2+}]_i$ at point *'B'*	12.3 ± 3	14.5 ± 2.2*	10.6 ± 1.9*	11.8 ± 1.6#
Active force / $\Delta [Ca^{2+}]_i$ at point *'C'*	32.6 ± 5	53.1 ± 8.6*	28.1 ± 4.5*	30.1 ± 3.9#

Unit: $mN \cdot mm^{-2} \cdot \mu M^{-1}$.

* $p < 0.05$ vs control;

# $p < 0.05$ vs FN alone.